

High-temperature superconductivity of $Pm\bar{3}n$ Lu_4H_{23} immersed in an as-synthesized lutetium polyhydride

Xiaoming Zhang ^{1,*}, Zheng Liu ², and Feng Liu³

¹College of Physics and Optoelectronic Engineering, Ocean University of China, Qingdao, Shandong 266100, China

²Institute for Advanced Study, Tsinghua University, Beijing 100084, China

³Department of Materials Science and Engineering, University of Utah, Salt Lake City, Utah 84112, USA



(Received 15 November 2023; revised 27 May 2024; accepted 6 June 2024; published 20 June 2024)

The precompression effect of foreign elements affords a promising route to metallizing hydrogen atoms under moderate pressure and achieving superconductivity with high transition temperature (T_C) in polyhydrides. Recently, lutetium (Lu) polyhydrides are receiving considerable attention due to their fully filled f orbitals, which are favorable for realizing high T_C . The highest T_C observed in the as-synthesized lutetium polyhydrides up to now has reached 65–71 K under pressures of 181–218 GPa, which was attributed to the $Pm\bar{3}n$ Lu_4H_{23} phase but without computational analysis. Here we perform first-principles calculations on the bonding feature, the stability, the electronic property, and the superconductivity of Lu_4H_{23} . Lu_4H_{23} presents robust metallicity due to the orbital hybridizations associated with the H-H covalent and Lu-H ionic bonds, as well as the charge transfer from Lu to H atoms. Our calculations reveal that Lu_4H_{23} can be stabilized at pressures above ~ 200 GPa, whose T_C is estimated to be 69–225 (103–210) K at 200 (218) GPa and maintains at the average values around 150–200 K under the pressures exceeding 250 GPa. We propose that the $Fm\bar{3}m$ LuH plays a possible role in stabilizing Lu_4H_{23} at pressures lower than 200 GPa, and, simultaneously, decreases the T_C of superconductivity in the as-synthesized lutetium polyhydrides. Our work provides a computational analysis on Lu_4H_{23} , and the predicted high T_C is expected to be experimentally realized by increasing pressure and optimizing synthesis process to eliminate the LuH phase.

DOI: [10.1103/PhysRevB.109.224511](https://doi.org/10.1103/PhysRevB.109.224511)

I. INTRODUCTION

Since first discovered by Onnes in 1911, superconductivity (SC) has received continuous and extensive research attention in the fields of condensed matter physics and material science. Increasing the transition temperature (T_C) of SC is one ambitious motivation in pursuing novel SC candidates. It was theoretically proposed that metallic hydrogen (H) with high Debye temperature and strong electron-phonon coupling (EPC) is promising in realizing high- T_C SC within the framework of the Bardeen-Cooper-Schrieffer theory [1–4]. However, the formation of metallic hydrogen demands extremely high pressure, ~ 500 GPa [5], which is still a great challenge and impractical for application. The chemical precompression effect of foreign elements provides a possible route to decrease pressure [6], as evidenced by discovering the SC of hydrogen sulfide with $T_C = 203$ K under 155 GPa [7–10].

Rare-earth polyhydrides with clathratelike structure [11], such as Sc-H [12,13], Y-H [14,15], La-H [16], Ac-H [17], Ce-H [18], Th-H [19], and La-Y-H [20] systems, represent a large material family with high- T_C SC. The T_C of $Fm\bar{3}m$ LaH_{10} was initially predicted to be 274–286 K under 210 GPa [21] and then experimentally confirmed with $T_C = 250 - 260$ K under 170–180 GPa [22,23]. Subsequent experiments show the $Fm\bar{3}m$ LaH_{10} can be decompression transformed to C_2/m

phase at critical pressures of around 138–160 GPa [24,25], which results in a steep variation of T_C below and a slow variation above the critical pressure. The high T_C of LaH_{10} is attributed to the non-neglectable density of states (DOS) of the H atom at the Fermi level E_F [26] and the unfilled f shells of the La atom located at the beginning of the lanthanide series [27]. This fact provokes the prediction of high- T_C SC in the polyhydrides of later lanthanides with fully filled f shells [28], such as the $Im\bar{3}m$ LuH_6 with $T_C = 273$ K at 100 GPa [29] and the $Immm$ LuH_6 with $T_C = 86.2$ K at 300 GPa [30]. Experimentally, in addition to the identified SC with $T_C \sim 12.4$ K of $Fm\bar{3}m$ LuH_3 at 122 GPa [12], the SC of lutetium polyhydride with $T_C = 65 - 71$ K was observed under the pressure of 181–218 GPa [31]. The *in situ* high-pressure x-ray diffraction (XRD) experiments imply the as-synthesized lutetium polyhydride containing $Pm\bar{3}n$ Lu_4H_{23} and $Fm\bar{3}m$ LuH, where the former was proposed to be responsible for the observed SC but without further computational analysis [31].

Computational analysis based on density functional theory provides a powerful tool not only in predicting high- T_C polyhydrides, but also in interpreting experimental results. Recently, a paper that falsely reported near-ambient SC with $T_C = 273$ K in a nitrogen-doped lutetium hydride (Lu-N-H) was retracted [32], which, on the other hand, led to notable research attention on the fluorite-type LuH_2 with $Fm\bar{3}m$ crystal symmetry. The $Fm\bar{3}m$ LuH_2 was computationally proposed to be the dominant component of the Lu-N-H system based on constructing a Lu-N-H phase diagram as well as simulating optical absorption spectra and XRD patterns

*Contact author: zxm@ouc.edu.cn

[33–37], which is in good agreement with the conclusion of related experiments and the observed color changes under pressure [38–42]. Furthermore, the absence of SC under near-ambient pressure in the $Fm\bar{3}m$ LuH_2 was consistently revealed by both computational [35–37] and experimental reports [40–43].

In this paper, we provide a computational insight into the bonding feature, the stability, the electronic property, and the SC of $Pm\bar{3}n$ Lu_4H_{23} . Our calculations indicate that the $Pm\bar{3}n$ Lu_4H_{23} can be stabilized under pressures higher than 200 GPa, and the stable $Fm\bar{3}m$ LuH phase plays the role of stabilizing the $Pm\bar{3}n$ Lu_4H_{23} in the as-synthesized lutetium polyhydride under pressures lower than 200 GPa [31]. The metallicity of the $Pm\bar{3}n$ Lu_4H_{23} stems from the orbital hybridizations and the charge transfer between the Lu and H atoms, which enables the precondition of emerging SC with high T_C . The estimated T_C is 103–210 K at 218 GPa and changes to 69–225 K at 200 GPa, where the low limit of T_C approaches the experimentally reported $T_C = 65 - 71$ K at 181–218 GPa in the as-synthesized lutetium polyhydride [31]. We attribute the non-negligible deviation of T_C to the existence of the $Fm\bar{3}m$ LuH phase with low T_C in the as-synthesized samples. The average T_C of Lu_4H_{23} is around 150–200 K when the pressures exceed 250 GPa, which is expected to be experimentally realized by optimizing the synthesis process to eliminate the LuH phase.

II. RESULTS AND DISCUSSIONS

A. The bonding feature, stability, and electronic property of Lu_4H_{23}

The $Pm\bar{3}n$ Lu_4H_{23} adopts the structure of Weaire-Phelan foam, which is stacked by the clathrates with 12 or 14 facets [Fig. 1(a)]. The clathrate with 12 facets is constructed by 20 H atoms and the facets are all pentagons, while the clathrate with 14 facets consists of 24 H atoms and the 14 facets include 2 hexagons and 10 pentagons. The 20 H clathrates are separated by the 24 H clathrates, and the 24 H clathrates connect with each other by sharing edges or hexagonal facets. Each clathrate encases one Lu atom [Fig. 1(a)]. The Lu atoms within the 20 H clathrates occupy the corner or center of the $Pm\bar{3}n$ Lu_4H_{23} primitive cell, and the Lu atoms within the 24 H clathrates locate at the faces of the Lu_4H_{23} primitive cell. The bonding feature, the stability, and the electronic property of Lu_4H_{23} were investigated by using the QUANTUM ESPRESSO (QE) package [44] and the Vienna *Ab initio* simulation package [45], where the computational details are presented in Sec. I of the Supplemental Material (SM) [46], which includes Refs. [31,44,45,47–60].

The crystal structure of the $Pm\bar{3}n$ Lu_4H_{23} was fully optimized under different pressures and our calculated results indicate the van der Waals interaction is necessary to reproduce the experimentally reported lattice constant a of the $Pm\bar{3}n$ Lu_4H_{23} at 185 GPa [upper panel of Fig. 1(b)], which gradually decreases with the increase of pressure. The bonding feature is investigated by analyzing the H-H bond lengths (d_H), the distribution of electron localization function (ELF), and the crystal orbital Hamiltonian population (COHP). Most of the H-H bonds in Lu_4H_{23} have lengths shorter than

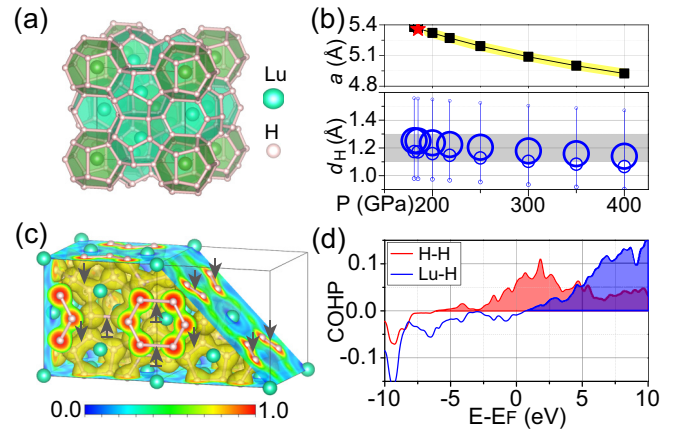


FIG. 1. (a) The crystal structure of $Pm\bar{3}n$ Lu_4H_{23} . (b) Upper panel: the calculated lattice constants a of Lu_4H_{23} under different pressures, where the red star denotes the experimentally reported lattice constant at 185 GPa. Lower panel: the variation of H-H bond lengths d_H under different pressures, and the number of bonds with a given length is drawn proportionally to the magnitude of the circle. (c) The ELF distributions of Lu_4H_{23} at 218 GPa, where the value of ELF on the cutting planes is represented by color and the isosurface of ELF is set to 0.5. The H-H bonds with the length being longer than 1.3 Å and shorter than 1.1 Å are respectively marked by upward and downward arrows, while the H-H bonds without marked arrows have the length between 1.1 and 1.3 Å. (d) The calculated COHP for the H-H and Lu-H bonds of the $Pm\bar{3}n$ Lu_4H_{23} at 218 GPa.

1.3 Å but longer than 1.1 Å [lower panel of Fig. 1(b)], which present weak covalent bonding interaction as indicated by the associated ELF value of ~ 0.6 [Fig. 1(c)]. The H-H bonds with lengths shorter than 1.0 Å connect the 20 H clathrates along the diagonal direction of the Lu_4H_{23} primitive cell, which is a strong covalent bond with an ELF value exceeding 0.8 [Fig. 1(c)]. The length of H-H bonds longer than 1.3 Å corresponds to two parallel edges of the shared hexagonal facets between 24 H cages, which have ELF values smaller than 0.5 [Fig. 1(c)]. The ELF value between the Lu and H atoms is close to zero [Fig. 1(c)], suggesting their interactions are ionic bonding in nature. The COHP analysis [Fig. 1(d)] reveals that the states between H atoms are antibonding at the Fermi level as indicated by a positive COHP value, while the bonding states at the Fermi level between the Lu and H atoms are verified by a negative COHP value.

The dynamical stability of the $Pm\bar{3}n$ Lu_4H_{23} under the pressures up to 400 GPa was checked by calculating phonon spectra, which demonstrates the $Pm\bar{3}n$ Lu_4H_{23} is stable at pressures above 200 GPa, and a lower pressure will lead to imaginary frequency in acoustic modes [Fig. 2(a)]. The unstable phonon modes are closely related to the vibrations of Lu atoms along the direction parallel to the axis perpendicular to the shared hexagonal facets between 24 H cages. Specifically, the phonon instability around the Γ point stems from the shear modes [Fig. 2(b)] and that around the R point corresponds to the breathing modes [Fig. 2(c)], where the Lu atoms locating at the center of the 24 H cages play dominant roles on the phonon instability. The phonon instability may be the reason for the coexistence of $Pm\bar{3}n$ Lu_4H_{23} and $Fm\bar{3}m$ LuH in the as-synthesized lutetium polyhydride [31]. Phonon spectrum

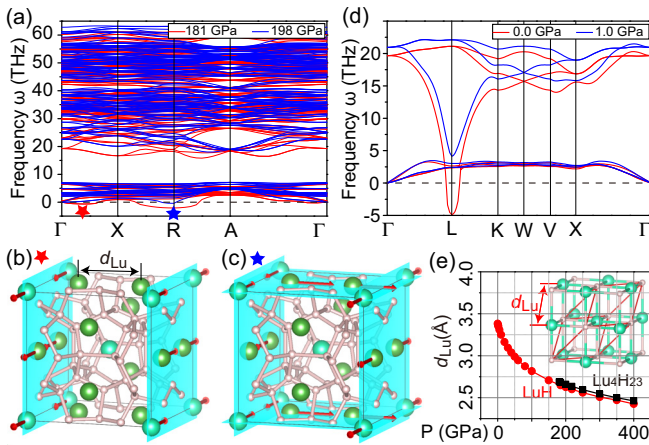


FIG. 2. (a) Phonon spectrum of the $Pm\bar{3}n$ Lu_4H_{23} at 181 (red lines) and 198 (blue lines) GPa. (b), (c) The vibrations of Lu atoms for the phonon modes with imaginary frequency marked by a (b) red and (c) blue star in the phonon spectrum plotted in (a). (d) Phonon spectrum of the $Fm\bar{3}m$ LuH at 0 (red lines) and 1 (blue lines) GPa. (e) The pressure-dependent distance between Lu atoms d_{Lu} marked in (b) and that marked in the inset of (e), which are respectively shown by black squares and red dots.

calculations indicate the $Fm\bar{3}m$ LuH can be stabilized by a pressure higher than 1 GPa [Fig. 2(d)], and the computational details based on the QE package [44] are also presented in Sec. I of the Supplemental Material (SM) [46]. Our analysis [Fig. 2(e)] shows that the distance between the Lu atoms encased by the 24 H cages [d_{Lu} , marked in Fig. 2(b)] is nearly equal to that [marked in the inset of Fig. 2(e)] of the $Fm\bar{3}m$ LuH. This fact may enable synthesizing the $Pm\bar{3}n$ Lu_4H_{23} from the $Fm\bar{3}m$ LuH, or vice versa, by sharing the Lu atoms with matched distance, and simultaneously, suppressing the phonon instability of the $Pm\bar{3}n$ Lu_4H_{23} when the pressure is lower than 200 GPa.

Next, the electronic band structure, DOS, and the charge density were calculated to reveal the metallicity of the $Pm\bar{3}n$ Lu_4H_{23} (Fig. 3). The metallic bands stem from the hybridization between H and Lu atoms [Fig. 3(a)], and the hybridized orbitals include the s and p orbitals of H atoms as well as the s , p , and d orbitals of Lu atoms [Fig. 3(b)]. The hybridization leads to seven Fermi surfaces with each Fermi surface possessing the contributions of both Lu and H atoms (Fig. S3 in the SM [46]). Figure 3(c) shows the distribution of partial charge density for the metallic states near the Fermi level. One can clearly see the Lu atoms within the 20 H clathrates hybridize to surrounded H atoms directly, while the hybridization between the rest of the Lu atoms and their surrounding 24 H atoms is indirect and the center of the shared hexagonal facets works as a bridging point. The latter with indirect hybridization may be one reason for the Lu atoms encased by 24 H clathrates emerging phonon instability first and foremost during decompression. The filling of s and p orbitals of H atoms with antibonding features is attributed to the charge transfer from Lu to H atoms. Bader charge analysis reveals that each Lu atom donates about one electron and each H atom accepts ~ 0.2 electron, which can be visualized from the distribution of charge density difference between

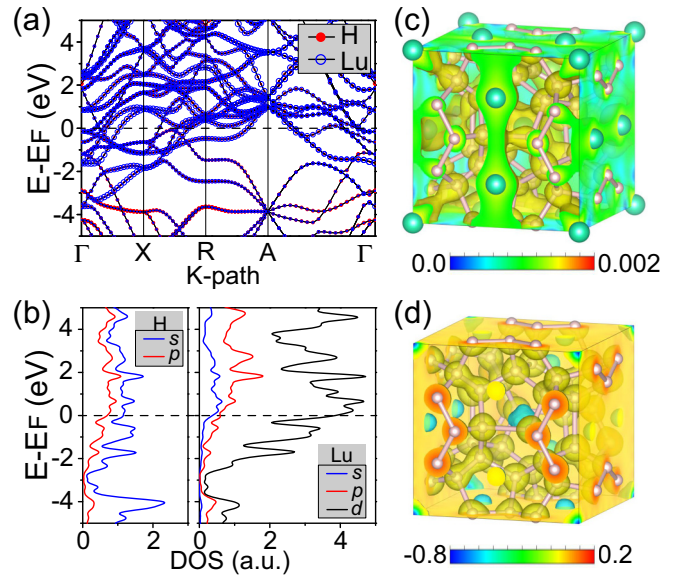


FIG. 3. (a) The atom-resolved band structure, (b) projected DOS, and (c) the distribution of partial charge density of the $Pm\bar{3}n$ Lu_4H_{23} at 218 GPa. The size of the red dot and blue circles in the band structure are respectively drawn proportional to the contribution of H and Lu atoms. The partial charge density is plotted for the metallic states with the energy ranging from $E_F - 10$ to $E_F + 10$ meV. (d) The distribution of the charge density difference between the self-consistent calculated charge density and the superposition of atomic charge density.

the self-consistent calculated results and the superposition of atomic charge density [Fig. 3(d)]. The blue isosurface around the location of the Lu atom indicates the loss of electrons, while the yellow isosurface surrounding the H atoms reveals the gain of electrons.

B. The SC of Lu_4H_{23}

The metallicity of the $Pm\bar{3}n$ Lu_4H_{23} provides the precondition of emerging phonon-mediated SC, and the non-neglectable DOS of H atoms at the Fermi level is favorable for enhancing T_C . The SC of the $Pm\bar{3}n$ Lu_4H_{23} was estimated by performing EPC calculation based on the QE package [44] (see details from Sec. II of the SM [46]). We present the phonon spectra of the $Pm\bar{3}n$ Lu_4H_{23} under 218 GPa in Fig. 4(a), which shows an obvious frequency gap around 10–20 THz. The phonon DOS $F(\omega)$ indicates that the gap separates the vibration of Lu from that of H atoms [Fig. 4(b)], with the former (latter) occupying a low (high) frequency range. This is attributed to the significant difference between the atomic mass of Lu and H atoms, whose motions tend to decouple with each other. The calculated isotropic Eliashberg function $\alpha^2F(\omega)$ presents similar peak structures with $F(\omega)$ [Fig. 4(b)]. This indicates that all phonon modes, i.e., the vibrations of both Lu and H atoms, participate in the process of electron-phonon scattering. Notably, one can see the $\alpha^2F(\omega)$ is significantly larger than the $F(\omega)$ when the frequency is higher than ~ 20 THz, while the $\alpha^2F(\omega)$ and $F(\omega)$ are comparable with each other at lower frequency. This indicates that the vibrations of H atoms enable strong electron-phonon

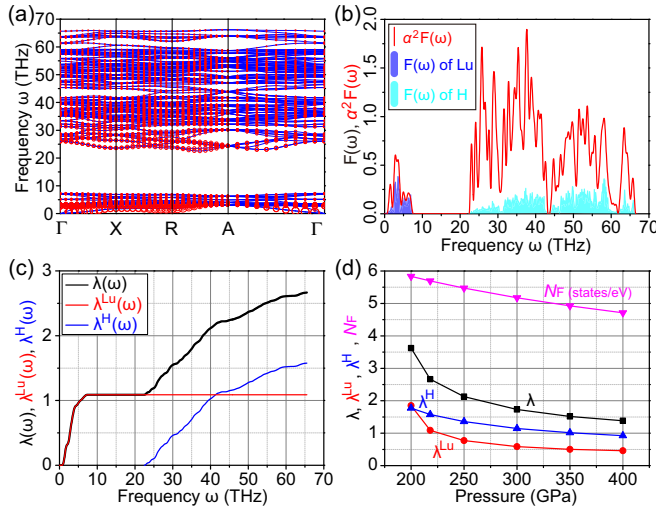


FIG. 4. (a) Phonon spectrum of the $Pm\bar{3}n$ Lu_4H_{23} at 218 GPa, where the size of the red circles is drawn proportional to the magnitude of the EPC $\lambda_{\mathbf{k}\nu}$. (b) The plot of the phonon DOS $F(\omega)$ and the Eliashberg spectral function $\alpha^2 F(\omega)$, where the $F(\omega)$ is resolved into the vibrations of Lu (blue region) and H (light-blue region) atoms. (c) The cumulative frequency-dependent $\lambda(\omega)$, $\lambda^{\text{Lu}}(\omega)$, and $\lambda^{\text{H}}(\omega)$ of Lu_4H_{23} at 218 GPa. (d) The variation of N_F , λ , λ^{Lu} , and λ^{H} of Lu_4H_{23} under different pressures, where the corresponding data are summarized in Table S2 of the SM [46].

interaction, which scatter electrons more significant than those of Lu atoms.

The cumulative frequency-dependent EPC function $\lambda(\omega)$ was then calculated based on the isotropic Eliashberg function $\alpha^2 F(\omega)$: $\lambda(\omega) = 2 \int_0^\omega d\omega' \frac{\alpha^2 F(\omega')}{\omega'}$. The $\lambda(\omega)$ is quickly increased by the vibrations of both Lu and H atoms [black line in Fig. 4(c)], leading to the total EPC $\lambda = 2.66$ for the Lu_4H_{23} at 218 GPa. The contributions of Lu and H atoms are $\lambda^{\text{Lu}} = 1.09$ and $\lambda^{\text{H}} = 1.58$, which are respectively evaluated by calculating the $\lambda^{\text{Lu}}(\omega)$ and $\lambda^{\text{H}}(\omega)$ from the isotropic Eliashberg function of Lu and H vibration modes solely [Fig. 4(c)]. In attrition to the comparable $\alpha^2 F(\omega)$ and $F(\omega)$ [Fig. 4(b)], the significant contribution of Lu atoms on the λ can be attributed to its low vibration frequency, i.e., phonon softening, because of the ω^{-1} scaling of $\lambda \sim \alpha^2 F(\omega)/\omega$. This fact can be captured from the momentum-resolved EPC $\lambda_{\mathbf{q}\nu}$ for a given phonon branch ν [Fig. 4(a)], where the $\lambda_{\mathbf{q}\nu}$ on the phonon modes of Lu is conspicuous. The strong EPC from the vibrations of H atoms can be understood in that the $\alpha^2 F(\omega)$ are significantly larger than its $F(\omega)$ [Fig. 4(b)], because most of the H-H bonds have intermediate lengths ranging from 1.1 to 1.3 Å [Fig. 1(b)] [61,62]. Similar analysis on the phonon spectra, the Eliashberg function $\alpha^2 F(\omega)$, and the EPC strength can be applied to the Lu_4H_{23} at 200 GPa (Fig. S4 in the SM [46]), 250 GPa (Fig. S5 in the SM [46]), 300 GPa (Fig. S6 in the SM [46]), 350 GPa (Fig. S7 in the SM [46]), and 400 GPa (Fig. S8 in the SM [46]).

The calculated EPC λ , λ^{Lu} , and λ^{H} of Lu_4H_{23} under different pressures are summarized in Fig. 4(d). Clearly, the total EPC λ is suppressed with the increase of pressure, which decreases rapidly, initially starting from 200 GPa, and then slows down when the pressure exceeds ~ 300 GPa. This trend can

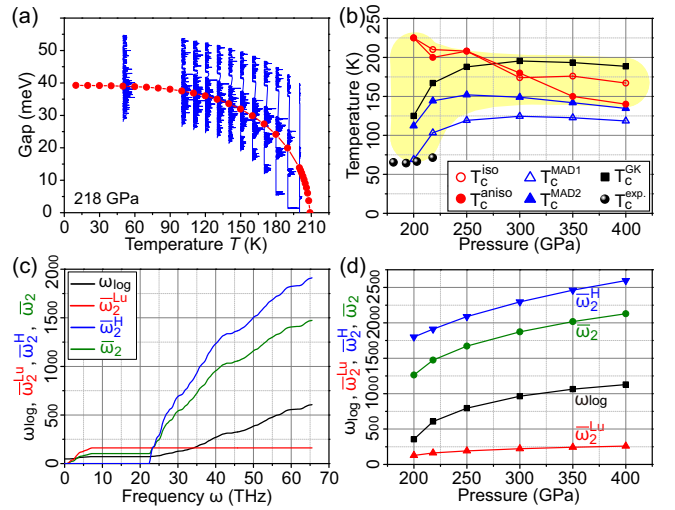


FIG. 5. (a) The temperature-dependent isotropic (red dots) and anisotropic (blue lines) superconducting gap for the Lu_4H_{23} under 218 GPa. (b) The summary of T_C calculated by using different methods for the Lu_4H_{23} under different pressures, where the yellow background represents a reasonable range for the T_C of Lu_4H_{23} . The black dots denote the experimentally reported T_C . (c) The cumulative frequency-dependent ω_{log} , $\bar{\omega}_2^{\text{Lu}}$, $\bar{\omega}_2^{\text{H}}$, and $\bar{\omega}_2$ of the $Pm\bar{3}n$ Lu_4H_{23} at 218 GPa. (d) The variation of ω_{log} , $\bar{\omega}_2$, $\bar{\omega}_2^{\text{Lu}}$, and $\bar{\omega}_2^{\text{H}}$ of Lu_4H_{23} under different pressures. The data used to plot figures (b) and (d) are summarized in Table S2 of the SM [46].

be understood from the simplified relation of EPC $\lambda = N_F V_{\text{ep}}$ [63], where the N_F is the DOS at Fermi level and the V_{ep} is the phonon-mediated pairing potential. The N_F decreases monotonically with the increase of pressure [Fig. 4(d)], because the reduced distances between H atoms [Fig. 1(b)], between Lu atoms [Fig. 2(e)], and between Lu and H atoms will enhance electron hopping and hence enlarge the band width. The pressure-dependent N_F is nearly parallel to the variation of λ for the pressure above 300 GPa, which indicates the EPC λ is mainly determined by the N_F while the V_{ep} remains intact in this pressure range. Differently, the increase of EPC λ is more and more rapid than that of N_F when pressure decreases from the 300 GPa. This indicates the dominant component that determines the strength of EPC changes from N_F to V_{ep} . The variations of λ^{Lu} and λ^{H} indicate that the greatly increased EPC at 200 GPa mainly stems from the vibrations of Lu atoms [Fig. 4(d)], due to the associated phonon softening providing an efficient route to enhancing the pairing potential V_{ep} .

Since the total EPC λ of the $Pm\bar{3}n$ Lu_4H_{23} under the considered pressures is around or even larger than 1.5 [Fig. 4(d)], representing a strong coupling limit, we evaluated the T_C of SC in the $Pm\bar{3}n$ Lu_4H_{23} by self-consistently calculating the leading edge of superconducting gaps at different temperatures, and the computational details based on the EPW (short name for electron-phonon Wannier) code [60] are presented in Sec. III of the SM [46]. For the Lu_4H_{23} under 218 GPa [Fig. 5(a)], the gaps evaluated from isotropic Migdal-Eliashberg equations are ~ 40 meV at zero temperature limit, which are gradually suppressed with the increase of temperature and vanish at the critical temperature of $T_C^{\text{iso}} = 210$ K. The energy distributions of the superconducting gap were

further calculated by solving anisotropic Migdal-Eliashberg equations. The obtained anisotropic gap varies from ~ 30 to ~ 50 meV at 50 K and closes at $T_C^{\text{aniso}} = 200$ K for the Lu_4H_{23} under 218 GPa [Fig. 5(a)]. Together with the self-consistently calculated gaps under different pressures (Fig. S9 [46]), we summarized the evaluated T_C^{iso} and T_C^{aniso} in Fig. 5(b), which indicate the Lu_4H_{23} holds the possibility of superconducting at the temperatures ranging from ~ 150 to ~ 200 K.

We further check the T_C of SC in the $Pm\bar{3}n$ Lu_4H_{23} by comprehensively considering the calculated results of the following McMillan-Allen-Dynes (MAD) [64,65] and Gor'kov-Kresin (GK) equations [66].

$$T_C^{\text{MAD1}} = \frac{\omega_{\text{log}}}{1.2} \exp\left[\frac{-1.04(1+\lambda)}{\lambda - \mu^*(1+0.62\lambda)}\right], \quad (1)$$

$$T_C^{\text{MAD2}} = f_1 f_2 T_C^{\text{MAD1}}, \quad (2)$$

$$T_C^{\text{GK}} = (\bar{\omega}_2^{\text{H}})^{\lambda^{\text{H}}/\lambda} (\bar{\omega}_2^{\text{Lu}})^{\lambda^{\text{Lu}}/\lambda} \exp\left(-\frac{1+\lambda}{\lambda - \mu^*}\right). \quad (3)$$

Here the Coulomb pseudopotential μ^* is set to 0.1. The logarithmically averaged frequency ω_{log} and the mean-square frequency $\bar{\omega}_2$ are respectively defined by $\omega_{\text{log}} = \exp\left[\frac{2}{\lambda} \int_0^\infty \frac{\alpha^2 F(\omega)}{\omega} \ln \omega d\omega\right]$ and $\bar{\omega}_2 = \sqrt{\frac{2}{\lambda} \int_0^\infty \alpha^2 F(\omega) \omega d\omega}$. It is known that the T_C^{MAD1} is valid for $\lambda \lesssim 1.5$, and the inclusion of $f_1 = [1 + (\frac{\lambda}{2.46(1+3.8\mu^*)})^{3/2}]^{1/3}$ and $f_2 = [1 + \frac{(\bar{\omega}_2/\omega_{\text{log}} - 1)\lambda^2}{\lambda^2 + [1.82(1+6.3\mu^*)\bar{\omega}_2/\omega_{\text{log}}]^2}]$ makes the T_C^{MAD2} reliable when $\lambda > 1.5$. T_C^{GK} is valid for $\lambda^{\text{H}} \approx \lambda^{\text{Lu}}$ [66], and the included mean-square frequencies $\bar{\omega}_2^{\text{H}}$ and $\bar{\omega}_2^{\text{Lu}}$ are calculated respectively from the isotropic Eliashberg function of Lu and H vibration modes solely. Note that the original T_C^{GK} were formulated for the candidates with well-separated optical and acoustic branches like the hydrogen sulfide [66]. The reason for substituting the EPC and the mean-square frequency of optical and acoustic branches by that of Lu and H atoms is that the phonon modes of more than one Lu atom in the $Pm\bar{3}n$ Lu_4H_{23} primitive cell can be regarded as folded acoustic branches [Fig. 4(a)].

These equations indicate the T_C of SC is not only dependent on the strength of EPC, but also on the logarithmically averaged frequency and the mean-square frequency. The cumulative frequency-dependent ω_{log} , $\bar{\omega}_2$, $\bar{\omega}_2^{\text{Lu}}$, and $\bar{\omega}_2^{\text{H}}$ for the Lu_4H_{23} under 218 GPa are plotted in Fig. 5(c). One can clearly see the ω_{log} contributed by the Lu atoms is only 71.9 K, being 11.9% of the total $\omega_{\text{log}} = 606.4$ K. The mean-square frequencies are calculated to $\bar{\omega}_2 = 1473.4$ K, $\bar{\omega}_2^{\text{Lu}} = 161.9$ K, and $\bar{\omega}_2^{\text{H}} = 1911.0$ K [Fig. 5(c)], respectively. These indicate the phonon modes of H atoms are more favorable for enhancing T_C than that of Lu atoms, consistent with the initial theory of realizing high- T_C SC from metallic hydrogen. Based on similar calculations on Lu_4H_{23} under 200 GPa [Fig. S4(d) in the SM [46]], 250 GPa [Fig. S5(d) in the SM [46]], 300 GPa [Fig. S6(d) in the SM [46]], 350 GPa [Fig. S7(d) in the SM [46]], and 400 GPa [Fig. S8(d) in the SM [46]], we obtained ω_{log} , $\bar{\omega}_2$, $\bar{\omega}_2^{\text{Lu}}$, and $\bar{\omega}_2^{\text{H}}$ under different pressures [Fig. 5(d)], which increase with increasing pressure. The T_C^{MAD1} , T_C^{MAD2} , and T_C^{GK} are then evaluated and also summarized in Fig. 5(b).

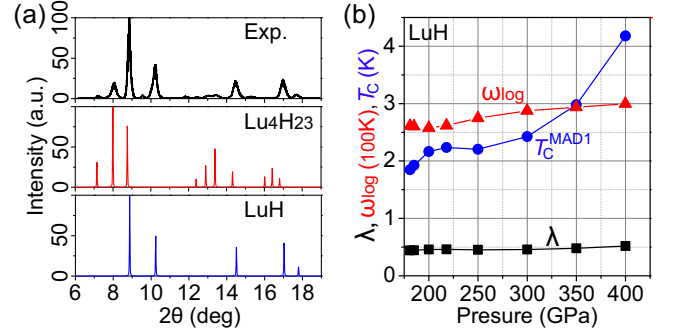


FIG. 6. (a) The comparison between the XRD patterns of as-synthesized lutetium polyhydride measured at 185 GPa (upper panel) [31] and the simulated XRD patterns for the fully relaxed $Pm\bar{3}n$ Lu_4H_{23} (middle panel) and $Fm\bar{3}m$ LuH (lower panel) under 185 GPa. (b) The variation of λ , ω_{log} , and T_C^{MAD1} of LuH under pressures ranging from 181 to 400 GPa.

Considering the conditions of the employed Eqs. (1)–(3) to be valid, one can expect the $Pm\bar{3}n$ Lu_4H_{23} to exhibit SC with T_C around 150–200 K when pressure is higher than 250 GPa, consistent with the results obtained by solving Migdal-Eliashberg equations. The T_C of Lu_4H_{23} ranges from ~ 69 (~ 103) to ~ 225 (~ 210) K under the pressure of 200 (218) GPa [Fig. 5(b)], where the low limit approaches the experimentally reported $T_C = 65 - 71$ K at 181–218 GPa in the as-synthesized lutetium polyhydride [31]. We highlight the reasonable range of T_C for the Lu_4H_{23} under different pressures by the yellow background in Fig. 5(b).

Lastly, we should point out that our estimated T_C for the $Pm\bar{3}n$ Lu_4H_{23} [Fig. 5(b)] are higher than the experimentally reported 65–71 K at 181–218 GPa in the as-synthesized lutetium polyhydride [31]. Since the SC of hydrides is highly sensitive to their symmetry and stoichiometry [24,25,67,68], the deviation can be attributed to the as-prepared sample containing the $Fm\bar{3}m$ LuH phase. By simulating XRD patterns under 185 GPa [31] can be reproduced by our fully relaxed $Pm\bar{3}n$ Lu_4H_{23} and $Fm\bar{3}m$ LuH under 185 GPa [Fig. 6(a)]. Notably, the XRD peak around $2\theta \sim 8^\circ$ is contributed solely by the $Pm\bar{3}n$ Lu_4H_{23} , which is low in the measured XRD pattern. This fact indicates the component of the $Pm\bar{3}n$ Lu_4H_{23} may be less in the as-synthesized lutetium polyhydride, and the dominant component should be $Fm\bar{3}m$ LuH. The calculated EPC of the $Fm\bar{3}m$ LuH is around 0.5 under pressures ranging from 181 to 400 GPa [Fig. 6(b)] and is unlikely to enable high- T_C SC, which is confirmed by the evaluated T_C^{MAD1} of being around 2 K at the pressures of 181–218 GPa and being lower than 4.5 K when the pressure increases from 218 to 400 GPa [Fig. 6(b)]. Consequently, one can expect to improve the T_C of lutetium polyhydrides by increasing the component of Lu_4H_{23} and eliminating the LuH phase starting from Ref. [31].

III. CONCLUSION

In this paper, we have performed comprehensive first-principles calculations on the bonding feature, the stability, the electronic property, and the SC of $Pm\bar{3}n$ Lu_4H_{23} and

$Fm\bar{3}m$ LuH. Our calculations indicate that both a H-H covalent bond and a Lu-H ionic bond exist in the $Pm\bar{3}n$ Lu₄H₂₃ with clathrate-like structure, while the $Fm\bar{3}m$ LuH only possesses Lu-H ionic bonds. The different bonding features make the $Pm\bar{3}n$ Lu₄H₂₃ stabilize under pressures higher than 200 GPa, but the LuH is stable once the pressure exceeds ~ 1 GPa. We propose that the LuH plays the role of stabilizing the $Pm\bar{3}n$ Lu₄H₂₃ in the as-synthesized lutetium polyhydride under pressures lower than 200 GPa [31], because the distance between the Lu atoms with phonon instability in Lu₄H₂₃ is well matched to that in LuH. The metallicity of the $Pm\bar{3}n$ Lu₄H₂₃ stems from the hybridization between the orbitals of H and Lu atoms, and the charge transfer from Lu to H atoms fills in the antibonding states between H atoms.

The SC of the $Pm\bar{3}n$ Lu₄H₂₃ is computationally revealed by calculating the EPC strength and estimating T_C . The EPC strength increases with the decrease of pressure, because the decompression softens phonon modes; it especially softens that of Lu vibrations. The T_C is estimated to be 69–225

(103–210) K under the pressure of 200 (218) GPa, where the low limit approaches the experimentally reported $T_C = 65 - 71$ K at 181–218 GPa in the as-synthesized lutetium polyhydride [31]. We attribute the non-negligible deviation of T_C to the presence of the $Fm\bar{3}m$ LuH phase with low T_C in the as-synthesized samples. The T_C of Lu₄H₂₃ is around 150–200 K at pressures ranging from 250 to 400 GPa, which are expected to be realized by increasing the component of Lu₄H₂₃ and eliminating the LuH phase through optimizing the synthesis process reported in Ref. [31].

ACKNOWLEDGMENTS

X.Z. acknowledges support from the National Natural Science Foundation of China (Grant No. 12004357). Z.L. acknowledges support from the National Natural Science Foundation of China (Grants No. 12374062 and No. 92365201). F.L. acknowledges support from DOE-BES (Grant No. DE-FG02-04ER46148).

-
- [1] N. W. Ashcroft, Metallic hydrogen: A high-temperature superconductor? *Phys. Rev. Lett.* **21**, 1748 (1968).
- [2] P. Cudazzo, G. Profeta, A. Sanna, A. Floris, A. Continenza, S. Massidda, and E. K. U. Gross, *Ab initio* description of high-temperature superconductivity in dense molecular hydrogen, *Phys. Rev. Lett.* **100**, 257001 (2008).
- [3] P. Cudazzo, G. Profeta, A. Sanna, A. Floris, A. Continenza, S. Massidda, and E. K. U. Gross, Electron-phonon interaction and superconductivity in metallic molecular hydrogen. I. Electronic and dynamical properties under pressure, *Phys. Rev. B* **81**, 134505 (2010).
- [4] P. Cudazzo, G. Profeta, A. Sanna, A. Floris, A. Continenza, S. Massidda, and E. K. U. Gross, Electron-phonon interaction and superconductivity in metallic molecular hydrogen. II. Superconductivity under pressure, *Phys. Rev. B* **81**, 134506 (2010).
- [5] R. P. Dias and I. F. Silvera, Observation of the Wigner-Huntington transition to metallic hydrogen, *Science* **355**, 715 (2017).
- [6] N. W. Ashcroft, Hydrogen dominant metallic alloys: High temperature superconductors? *Phys. Rev. Lett.* **92**, 187002 (2004).
- [7] A. P. Drozdov, M. I. Erements, I. A. Troyan, V. Ksenofontov, and S. I. Shylin, Conventional superconductivity at 203 kelvin at high pressures in the sulfur hydride system, *Nature (London)* **525**, 73 (2015).
- [8] D. Duan, Y. Liu, F. Tian, D. Li, X. Huang, Z. Zhao, H. Yu, B. Liu, W. Tian, and T. Cui, Pressure-induced metallization of dense (H₂S)₂H₂ with high- T_c superconductivity, *Sci. Rep.* **4**, 6968 (2014).
- [9] M. Einaga, M. Sakata, T. Ishikawa, K. Shimizu, M. I. Erements, A. P. Drozdov, I. A. Troyan, N. Hirao, and Y. Ohishi, Crystal structure of the superconducting phase of sulfur hydride, *Nat. Phys.* **12**, 835 (2016).
- [10] I. Errea, M. Calandra, C. J. Pickard, J. Nelson, R. J. Needs, Y. Li, H. Liu, Y. Zhang, Y. Ma, and F. Mauri, High-pressure hydrogen sulfide from first principles: A strongly anharmonic phonon-mediated superconductor, *Phys. Rev. Lett.* **114**, 157004 (2015).
- [11] D. Wang, Y. Ding, and H.-K. Mao, Future study of dense superconducting hydrides at high pressure, *Materials* **14**, 7563 (2021).
- [12] M. Shao, S. Chen, W. Chen, K. Zhang, X. Huang, and T. Cui, Superconducting ScH₃ and LuH₃ at megabar pressures, *Inorg. Chem.* **60**, 15330 (2021).
- [13] X. Ye, N. Zarifi, E. Zurek, R. Hoffmann, and N. W. Ashcroft, High hydrides of scandium under pressure: Potential superconductors, *J. Phys. Chem. C* **122**, 6298 (2018).
- [14] P. Kong, V. S. Minkov, M. A. Kuzovnikov, A. P. Drozdov, S. P. Besedin, S. Mozaffari, L. Balicas, F. F. Balakirev, V. B. Prakapenka, S. Chariton, D. A. Knyazev, E. Greenberg, and M. I. Erements, Superconductivity up to 243 K in the yttrium-hydrogen system under high pressure, *Nat. Commun.* **12**, 5075 (2021).
- [15] E. Snider, N. Dasenbrock-Gammon, R. McBride, X. Wang, N. Meyers, K. V. Lawler, E. Zurek, A. Salamat, and R. P. Dias, Synthesis of yttrium superhydride superconductor with a transition temperature up to 262 K by catalytic hydrogenation at high pressures, *Phys. Rev. Lett.* **126**, 117003 (2021).
- [16] D. Laniel, F. Trybel, B. Winkler, F. Knoop, T. Fedotenko, S. Khandarkhaeva, A. Aslandukova, T. Meier, S. Chariton, K. Glazyrin, V. Milman, V. Prakapenka, I. A. Abrikosov, L. Dubrovinsky, and N. Dubrovinskaia, High-pressure synthesis of seven lanthanum hydrides with a significant variability of hydrogen content, *Nat. Commun.* **13**, 6987 (2022).
- [17] D. V. Semenov, A. G. Kvashnin, I. A. Kruglov, and A. R. Oganov, Actinium hydrides AcH₁₀, AcH₁₂, and AcH₁₆ as high-temperature conventional superconductors, *J. Phys. Chem. Lett.* **9**, 1920 (2018).
- [18] X. Li, X. Huang, D. Duan, C. J. Pickard, D. Zhou, H. Xie, Q. Zhuang, Y. Huang, Q. Zhou, B. Liu, and T. Cui, Polyhydride CeH₉ with an atomic-like hydrogen clathrate structure, *Nat. Commun.* **10**, 3461 (2019).
- [19] D. V. Semenov, A. G. Kvashnin, A. G. Ivanova, V. Svitlyk, V. Y. Fominski, A. V. Sadakov, O. A. Sobolevskiy, V. M. Pudalov, I. A. Troyan, and A. R. Oganov, Superconductivity

- at 161 K in thorium hydride ThH₁₀: Synthesis and properties, *Mater. Today* **33**, 36 (2020).
- [20] D. V. Semenov, I. A. Troyan, A. G. Ivanova, A. G. Kvashnin, I. A. Kruglov, M. Hanfland, A. V. Sadakov, O. A. Sobolevskiy, K. S. Pervakov, I. S. Lyubutin, K. V. Glazyrin, N. Giordano, D. N. Karimov, A. L. Vasiliev, R. Akashi, V. M. Pudalov, and A. R. Oganov, Superconductivity at 253 K in lanthanum-yttrium ternary hydrides, *Mater. Today* **48**, 18 (2021).
- [21] H. Liu, I. I. Naumov, R. Hoffmann, N. W. Ashcroft, and R. J. Hemley, Potential high- T_c superconducting lanthanum and yttrium hydrides at high pressure, *Proc. Natl. Acad. Sci. USA* **114**, 6990 (2017).
- [22] M. Somayazulu, M. Ahart, A. K. Mishra, Z. M. Geballe, M. Baldini, Y. Meng, V. V. Struzhkin, and R. J. Hemley, Evidence for superconductivity above 260 K in lanthanum superhydride at megabar pressures, *Phys. Rev. Lett.* **122**, 027001 (2019).
- [23] A. P. Drozdov, P. P. Kong, V. S. Minkov, S. P. Besedin, M. A. Kuzovnikov, S. Mozaffari, L. Balicas, F. F. Balakirev, D. E. Graf, V. B. Prakapenka, E. Greenberg, D. A. Knyazev, M. Tkacz, and M. I. Eremets, Superconductivity at 250 K in lanthanum hydride under high pressures, *Nature (London)* **569**, 528 (2019).
- [24] Z. M. Geballe, H. Liu, A. K. Mishra, M. Ahart, M. Somayazulu, Y. Meng, M. Baldini, and R. J. Hemley, Synthesis and stability of lanthanum superhydrides, *Angew. Chem., Int. Ed.* **57**, 688 (2018).
- [25] D. Sun, V. S. Minkov, S. Mozaffari, Y. Sun, Y. Ma, S. Chariton, V. B. Prakapenka, M. I. Eremets, L. Balicas, and F. F. Balakirev, High-temperature superconductivity on the verge of a structural instability in lanthanum superhydride, *Nat. Commun.* **12**, 6863 (2021).
- [26] F. Peng, Y. Sun, C. J. Pickard, R. J. Needs, Q. Wu, and Y. Ma, hydrogen clathrate structures in rare earth hydrides at high pressures: Possible route to room-temperature superconductivity, *Phys. Rev. Lett.* **119**, 107001 (2017).
- [27] D. V. Semenov, D. Zhou, A. G. Kvashnin, X. Huang, M. Galasso, I. A. Kruglov, A. G. Ivanova, A. G. Gavriliuk, W. Chen, N. V. Tkachenko, A. I. Boldyrev, I. Troyan, A. R. Oganov, and T. Cui, Novel strongly correlated europium superhydrides, *J. Phys. Chem. Lett.* **12**, 32 (2021).
- [28] D. V. Semenov, I. A. Kruglov, I. A. Savkin, A. G. Kvashnin, and A. R. Oganov, On distribution of superconductivity in metal hydrides, *Curr. Opin. Solid State Mater. Sci.* **24**, 100808 (2020).
- [29] H. Song, Z. Zhang, T. Cui, C. J. Pickard, V. Z. Kresin, and D. Duan, High T_c superconductivity in heavy rare earth hydrides, *Chin. Phys. Lett.* **38**, 107401 (2021).
- [30] W. Sun, X. Kuang, H. D. J. Keen, C. Lu, and A. Hermann, Second group of high-pressure high-temperature lanthanide polyhydride superconductors, *Phys. Rev. B* **102**, 144524 (2020).
- [31] Z. Li *et al.*, Superconductivity above 70 K observed in lutetium polyhydrides, *Sci. China Phys. Mech.* **66**, 267411 (2023).
- [32] N. Dasenbrock-Gammon, E. Snider, R. McBride, H. Pasan, D. Durkee, N. Khalvashi-Sutter, S. Munasinghe, S. E. Dissanayake, K. V. Lawler, A. Salamat, and R. P. Dias, Retraction note: Evidence of near-ambient superconductivity in a N-doped lutetium hydride, *Nature (London)* **624**, 460 (2023).
- [33] F. Xie, T. Lu, Z. Yu, Y. Wang, Z. Wang, S. Meng, and M. Liu, Lu-H-N phase diagram from first-principles calculations, *Chin. Phys. Lett.* **40**, 057401 (2023).
- [34] M. Liu, X. Liu, J. Li, J. Liu, Y. Sun, X.-Q. Chen, and P. Liu, Parent structures of near-ambient nitrogen-doped lutetium hydride superconductor, *Phys. Rev. B* **108**, L020102 (2023).
- [35] K. P. Hilleke, X. Wang, D. Luo, N. Geng, B. Wang, F. Belli, and E. Zurek, Structure, stability, and superconductivity of N-doped lutetium hydrides at kbar pressures, *Phys. Rev. B* **108**, 014511 (2023).
- [36] P. P. Ferreira, L. J. Conway, A. Cucciari, S. Di Cataldo, F. Giannessi, E. Kogler, L. T. F. Eleno, C. J. Pickard, C. Heil, and L. Boeri, Search for ambient superconductivity in the Lu-N-H system, *Nat. Commun.* **14**, 5367 (2023).
- [37] X. Tao, A. Yang, S. Yang, Y. Quan, and P. Zhang, Leading components and pressure-induced color changes in N-doped lutetium hydride, *Sci. Bull.* **68**, 1372 (2023).
- [38] Y.-J. Zhang, X. Ming, Q. Li, X. Zhu, B. Zheng, Y. Liu, C. He, H. Yang, and H.-H. Wen, Pressure induced color change and evolution of metallic behavior in nitrogen-doped lutetium hydride, *Sci. China Phys., Mech. Astron.* **66**, 287411 (2023).
- [39] X. Zhao, P. Shan, N. Wang, Y. Li, Y. Xu, and J. Cheng, Pressure tuning of optical reflectivity in LuH₂, *Sci. Bull.* **68**, 883 (2023).
- [40] P. Shan, N. Wang, X. Zheng, Q. Qiu, Y. Peng, and J. Cheng, Pressure-induced color change in the lutetium dihydride LuH₂, *Chin. Phys. Lett.* **40**, 046101 (2023).
- [41] X. Ming, Y.-J. Zhang, X. Zhu, Q. Li, C. He, Y. Liu, T. Huang, G. Liu, B. Zheng, H. Yang, J. Sun, X. Xi, and H.-H. Wen, Absence of near-ambient superconductivity in LuH_{2±x}N_y, *Nature (London)* **620**, 72 (2023).
- [42] X. Xing, C. Wang, L. Yu, J. Xu, C. Zhang, M. Zhang, S. Huang, X. Zhang, Y. Liu, B. Yang, X. Chen, Y. Zhang, J. Guo, Z. Shi, Y. Ma, C. Chen, and X. Liu, Observation of non-superconducting phase changes in nitrogen doped lutetium hydrides, *Nat. Commun.* **14**, 5991 (2023).
- [43] S. Cai, J. Guo, H. Shu, L. Yang, P. Wang, Y. Zhou, J. Zhao, J. Han, Q. Wu, W. Yang, T. Xiang, H.-k. Mao, and L. Sun, No evidence of superconductivity in a compressed sample prepared from lutetium foil and H₂/N₂ gas mixture, *Matter Radiat. Extremes* **8**, 048001 (2023).
- [44] P. Giannozzi, O. Basergio, P. Bonfà, D. Brunato, R. Car, I. Carnimeo, C. Cavazzoni, S. de Gironcoli, P. Delugas, F. Ferrari Ruffino, A. Ferretti, N. Marzari, I. Timrov, A. Urru, and S. Baroni, Quantum ESPRESSO toward the exascale, *J. Chem. Phys.* **152**, 154105 (2020).
- [45] G. Kresse and J. Furthmüller, Efficiency of ab-initio total energy calculations for metals and semiconductors using a plane-wave basis set, *Comput. Mater. Sci.* **6**, 15 (1996).
- [46] See Supplemental Material at <http://link.aps.org/supplemental/10.1103/PhysRevB.109.224511> for details of first-principles calculations, supplemental figures, and supplemental tables.
- [47] P. Hohenberg and W. Kohn, Inhomogeneous electron gas, *Phys. Rev.* **136**, B864 (1964).
- [48] W. Kohn and L. J. Sham, Self-consistent equations including exchange and correlation effects, *Phys. Rev.* **140**, A1133 (1965).
- [49] J. P. Perdew, K. Burke, and M. Ernzerhof, Generalized gradient approximation made simple, *Phys. Rev. Lett.* **77**, 3865 (1996).
- [50] S. Baroni, S. de Gironcoli, A. Dal Corso, and P. Giannozzi, Phonons and related crystal properties from density-functional perturbation theory, *Rev. Mod. Phys.* **73**, 515 (2001).

- [51] P. E. Blöchl, Projector augmented-wave method, *Phys. Rev. B* **50**, 17953 (1994).
- [52] S. Maintz, V. L. Deringer, A. L. Tchougréeff, and R. Dronskowski, LOBSTER: A tool to extract chemical bonding from plane-wave based DFT, *J. Comput. Chem.* **37**, 1030 (2016).
- [53] K. Momma and F. Izumi, VESTA 3 for three-dimensional visualization of crystal, volumetric and morphology data, *J. Appl. Crystallogr.* **44**, 1272 (2011).
- [54] M. Kawamura, FermiSurfer: Fermi-surface viewer providing multiple representation schemes, *Comput. Phys. Commun.* **239**, 197 (2019).
- [55] P. B. Allen, Neutron spectroscopy of superconductors, *Phys. Rev. B* **6**, 2577 (1972).
- [56] A. B. Migdal, Interaction between electrons and lattice vibrations in a normal metal, *Sov. Phys. JETP USSR* **7**, 996 (1958).
- [57] G. M. Eliashberg, Interactions between electrons and lattice vibrations in a superconductor, *Sov. Phys. JETP USSR* **11**, 696 (1960).
- [58] E. R. Margine and F. Giustino, Anisotropic Migdal-Eliashberg theory using Wannier functions, *Phys. Rev. B* **87**, 024505 (2013).
- [59] N. Marzari, A. A. Mostofi, J. R. Yates, I. Souza, and D. Vanderbilt, Maximally localized Wannier functions: Theory and applications, *Rev. Mod. Phys.* **84**, 1419 (2012).
- [60] S. Poncé, E. R. Margine, C. Verdi, and F. Giustino, EPW: Electron-phonon coupling, transport and superconducting properties using maximally localized Wannier functions, *Comput. Phys. Commun.* **209**, 116 (2016).
- [61] M. Du, H. Song, Z. Zhang, D. Duan, and T. Cui, Room-temperature superconductivity in Yb/Lu substituted clathrate hexahydrides under moderate pressure, *Research* **2022**, 9784309 (2022).
- [62] F. Belli, T. Novoa, J. Contreras-García, and I. Errea, Strong correlation between electronic bonding network and critical temperature in hydrogen-based superconductors, *Nat. Commun.* **12**, 5381 (2021).
- [63] C. Si, Z. Liu, W. Duan, and F. Liu, First-principles calculations on the effect of doping and biaxial tensile strain on electron-phonon coupling in graphene, *Phys. Rev. Lett.* **111**, 196802 (2013).
- [64] W. L. McMillan, Transition temperature of strong-coupled superconductors, *Phys. Rev.* **167**, 331 (1968).
- [65] P. B. Allen and R. C. Dynes, Transition temperature of strong-coupled superconductors reanalyzed, *Phys. Rev. B* **12**, 905 (1975).
- [66] L. P. Gor'kov and V. Z. Kresin, *Colloquium*: High pressure and road to room temperature superconductivity, *Rev. Mod. Phys.* **90**, 011001 (2018).
- [67] I. Errea, M. Calandra, C. J. Pickard, J. R. Nelson, R. J. Needs, Y. Li, H. Liu, Y. Zhang, Y. Ma, and F. Mauri, Quantum hydrogen-bond symmetrization in the superconducting hydrogen sulfide system, *Nature (London)* **532**, 81 (2016).
- [68] V. S. Minkov, V. B. Prakapenka, E. Greenberg, and M. I. Eremets, A boosted critical temperature of 166 K in superconducting D₃S synthesized from elemental sulfur and hydrogen, *Angew. Chem., Int. Ed.* **59**, 18970 (2020).